

Towards Microscopic Ab Initio Calculations of Astrophysical S -Factors[†]

Thomas Neff, Hans Feldmeier and Karlheinz Langanke
GSI Helmholtzzentrum für Schwerionenforschung GmbH
Planckstraße 1, 64291 Darmstadt, Germany

Abstract

Low energy capture cross sections are calculated within a microscopic many-body approach using an effective Hamiltonian derived from the Argonne V18 potential. The dynamics is treated within Fermionic Molecular Dynamics (FMD) which uses a Gaussian wave-packet basis to represent the many-body states. A phase-shift equivalent effective interaction derived within the Unitary Correlation Operator Method (UCOM) that treats explicitly short-range central and tensor correlations is employed. As a first application the ${}^3\text{He}(\alpha,\gamma){}^7\text{Be}$ reaction is presented. Within the FMD approach the microscopic many-body wave functions of the $3/2^-$ and $1/2^-$ bound states in ${}^7\text{Be}$ as well as the many-body scattering states in the $1/2^+$, $3/2^+$ and $5/2^+$ channels are calculated as eigenstates of the same microscopic effective Hamiltonian. Finally the S -factor is calculated from $E1$ transition matrix elements between the many-body scattering and bound states. For ${}^3\text{He}(\alpha,\gamma){}^7\text{Be}$ the S factor agrees very well, both in absolute normalization and energy dependence, with the recent experimental data from the Weizmann, LUNA, Seattle and ERNA experiments. For the ${}^3\text{H}(\alpha,\gamma){}^7\text{Li}$ reaction the calculated S -factor is about 15% above the data.

1 Introduction

Low energy nuclear reactions play an important role in many astrophysical scenarios. If the environmental temperature is so low that the kinetic energy of the nuclei is small compared to the Coulomb barrier, quantum tunneling leads to reaction rates which are exponentially dropping with decreasing energy. Hence it becomes increasingly difficult to impossible to measure the tiny cross sections at such small energies and one has often to rely on extrapolations to astrophysically relevant energies. Typically these reactions are described with potential models where the reaction partners are treated as point-like nuclei interacting via nucleus-nucleus potentials fitted to experimental data on bound and scattering states. In a microscopic *ab initio* picture however, the system is regarded as a many-body system of interacting nucleons. The many-body wave functions are fully antisymmetrized and realistic nucleon-nucleon interactions are used.

In the Fermionic Molecular Dynamics (FMD) approach [1, 2, 3, 4] we aim at a consistent description of bound states, resonances and scattering states using realistic low-momentum nucleon-nucleon interactions obtained in the Unitary Correlation Operator Method (UCOM) [5, 6, 7, 8, 9]. Intrinsic many-body basis states are Slater determinants built with Gaussian wave packets as single-particle states. This basis contains as special cases harmonic oscillator shell model and Brink-type cluster wave functions. The symmetries of the system are restored by projection on parity, angular momentum and

total linear momentum. The many-body eigenstates of the realistic Hamiltonian are obtained in multi-configuration mixing calculations. FMD has already been used successfully to describe the structure of nuclei in the p - and sd -shell, like the Hoyle state in ^{12}C [10] or halo- and cluster-structures in Neon isotopes [11].

In this contribution we extend FMD to the continuum where many-body states have to be matched to phase shifted Coulomb solutions of point like nuclei. We present first results for the $^3\text{He}(\alpha,\gamma)^7\text{Be}$ and $^3\text{H}(\alpha,\gamma)^7\text{Li}$ capture cross sections using the FMD approach. The $^3\text{He}(\alpha,\gamma)^7\text{Be}$ reaction, which is the onset of the ^7Be and ^8B branches of the pp II and pp III chain of hydrogen burning, has been studied theoretically since long either using potential models [12, 13] or microscopic cluster models [14, 15] assuming $^3\text{He}+^4\text{He}$ cluster wave functions. Polarization effects were considered by including the $^6\text{Li}+p$ channel in [16, 17]. However, consistent *ab initio* calculations starting from realistic interactions have not been possible up to now. First attempts using Variational Monte-Carlo [18] and the No-Core Shell Model [19] only calculated the asymptotic normalization coefficients from the bound state wave functions.

2 Fermionic Molecular Dynamics

In FMD the intrinsic many-body basis states are Slater determinants

$$|Q\rangle = \mathcal{A}\{|q_1\rangle \otimes \dots \otimes |q_A\rangle\}, \quad (1)$$

using Gaussian wave packets as single-particle states

$$\langle \vec{x}|q_k\rangle = \exp\left\{-\frac{(\vec{x} - \vec{b}_k)^2}{2a_k}\right\} \otimes |\chi_k^\uparrow, \chi_k^\downarrow\rangle \otimes |\xi_k\rangle. \quad (2)$$

The variational set Q contains the complex parameters \vec{b}_k , which encode the mean positions and momenta of the wave packets, the complex width parameters a_k , and the spin directions are controlled by χ_k^\uparrow and χ_k^\downarrow . Proton and neutron are distinguished by ξ_k . To restore the symmetries of the Hamiltonian the intrinsic wave function $|Q\rangle$ is projected on parity, angular momentum and total linear momentum $\vec{P} = 0$.

$$|Q; J^\pi MK\rangle \otimes |\vec{P} = 0\rangle_{cm} = P_{MK}^J P^\pi P^{\vec{P}=0} |Q\rangle \quad (3)$$

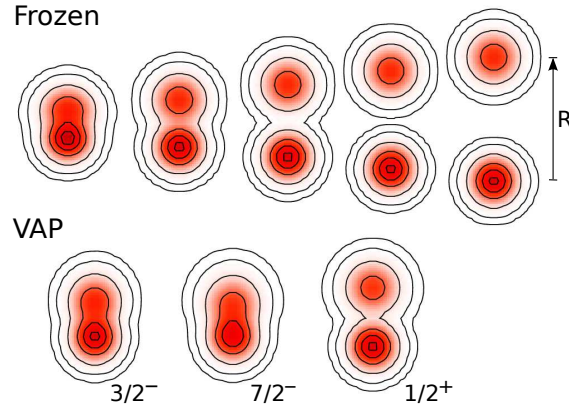


Figure 1: Density distributions of the intrinsic basis states. Top: frozen cluster configurations, bottom: selected polarized configurations obtained by Variation After parity and angular momentum Projection.

We divide the Hilbert space into an outer region where the system is represented as ${}^3\text{He}$ and ${}^4\text{He}$ nuclei in their ground states interacting only via the Coulomb interaction. In the inner region the nuclear force acts among all nucleons and the strong interactions between the approaching nuclei will polarize them. Therefore one has to enlarge the many-body Hilbert space beyond the microscopic cluster model [20] where the Hilbert space is spanned by so called “frozen” configurations that are just antisymmetrized products of the ${}^4\text{He}$ and ${}^3\text{He}$ clusters in their ground state placed at various distances R , see Fig. 1.

In order account for polarized clusters we generate additional configurations by a variation after parity and angular momentum projection procedure (VAP). The energy of the projected many-body state is minimized with respect to the parameters of all single particle states of the intrinsic Slater determinant in the sub-manifold defined by a fixed mean square radius. By dialing the value of the radius constraint from large to small we obtain polarized clusters down to shell model like configurations. The polarized clusters are essential for the continuum scattering states and the surface region of the bound states. The shell model like configurations contribute mainly to bound states. Some polarized configurations are shown in Fig. 1 (VAP). The many-body Hilbert space is spanned by the non-orthogonal projected configurations given in Eq. (3). The task is to find a set of intrinsic states $|Q^{(a)}\rangle$ that describes the physics well. Typically, we employ of the order of 50 intrinsic states which are taken to be the same set for bound and scattering states, of course projected on the respective J^π .

The effective Hamiltonian is diagonalized in the available Hilbert space with the proper boundary conditions for either bound (discrete values of the energy E_n) or scattering states ($E = k^2/(2\mu)$).

$$H^{\text{eff}} |J^\pi M, E_n\rangle = E_n |J^\pi M, E_n\rangle \quad (4)$$

This determines the multi-configuration mixing coefficients $c_{aK}^{(n)}$ of the microscopic many-body eigenstates

$$|J^\pi M, E_n\rangle = \sum_{aK} c_{aK}^{(n)} |Q^{(a)}; J^\pi MK\rangle . \quad (5)$$

The effective Hamiltonian $H^{\text{eff}} = T + V_{\text{UCOM}}$ is obtained within the Unitary Correlation Operator Method (UCOM) by transforming the realistic Argonne-V18 Hamiltonian in the two-body space [5]. This incorporates the short-range correlations into the effective interaction V_{UCOM} and at the same time leaves the phase shifts of the nucleon-nucleon scattering problem and the deuteron energy unchanged.

3 Bound and Scattering States

The frozen states can be rewritten using RGM basis states [21, 22].

$$|\Phi(r); [\ell \frac{1}{2}^+]_M^{J^\pi}\rangle = \mathcal{A} \left[|r, \ell\rangle_{rel} \otimes |{}^3\text{He}; \frac{1}{2}^+\rangle \otimes |{}^4\text{He}; 0^+\rangle \right]_M^{J^\pi} , \quad (6)$$

where $|r, \ell\rangle_{rel}$ denotes a state of relative motion with angular momentum ℓ in which the center of masses of the internal ground states $|{}^3\text{He}; \frac{1}{2}^+\rangle$ and $|{}^4\text{He}; 0^+\rangle$ are positioned at relative distance r . Internal and relative motion angular momenta are coupled to total J . The RGM representation can then be used to match the logarithmic derivative of the relative wave function of the clusters to the asymptotic Whittaker function for bound states or to Coulomb scattering wave functions with phase shifts:

$$\langle \Phi(r); [\ell \frac{1}{2}^+]_M^{J^\pi} | J^\pi M, E \rangle \xrightarrow{r \rightarrow \infty} \frac{1}{r} \left(F_\ell(kr) + \tan(\delta_\ell^{J^\pi}(k)) G_\ell(kr) \right), \quad k = +\sqrt{2\mu E} . \quad (7)$$

Using the microscopic R -matrix approach of the Brussels group [21, 22] we solve the Schrödinger equation with the proper boundary conditions for bound and scattering states.

With frozen configurations alone the $3/2^-$ and $1/2^-$ states in ${}^7\text{Be}$ are bound by only 240 keV and 10 keV, respectively. In the full Hilbert space, including the polarized configurations, we obtain binding energies of 1.49 MeV and 1.31 MeV with respect to the cluster threshold. In other words we reproduce the centroid energy but underestimate the splitting of the $3/2^-$ and $1/2^-$ states. By artificially increasing the spin-orbit strength we observed that the total cross section depends essentially only on the centroid energy while the increased splitting affects only the branching slightly. The calculated ${}^7\text{Be}$ charge radius of 2.67 fm is in good agreement with the experimental value of 2.647(17) fm [23]. In Fig. 2 we present the calculated phase shifts together with the experimental data [24]. Again we see a sizable effect when we compare the results using only the frozen configurations with the results obtained in the full Hilbert space including polarization effects.

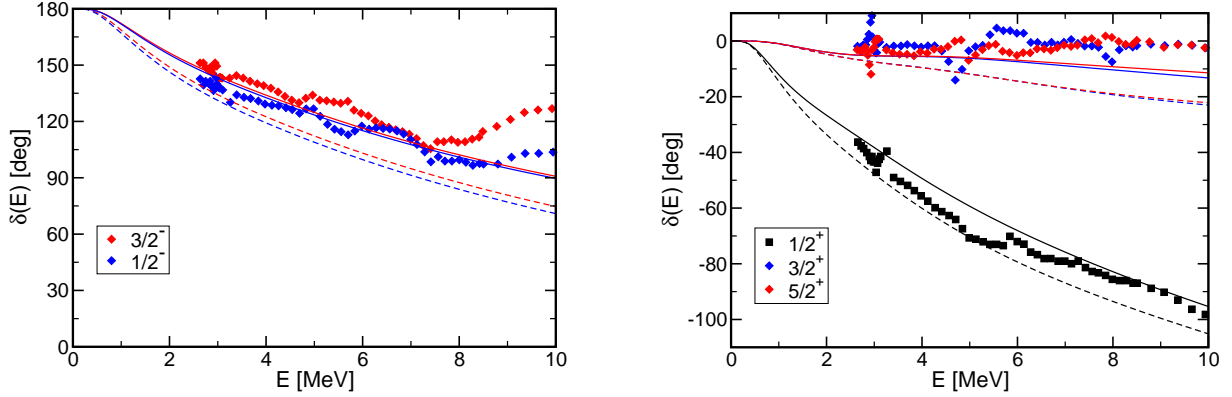


Figure 2: ${}^4\text{He} + {}^3\text{He}$ scattering phase shifts for P -waves left and the S and D -waves right. Dashed lines show results using only frozen cluster configurations, solid lines show results for the full model space.

4 Spectroscopic amplitudes

If the many-body system has a pronounced cluster structure, as is the case in ${}^7\text{Li}$, one can define an overlap function $\hat{\psi}_E^{J^\pi}(r)$ for the relative motion of the clusters by means of the spectroscopic amplitude $\langle \Phi(r) | J^\pi, E \rangle \equiv \langle \Phi(r); [\ell \frac{1}{2}^+]_M^{J^\pi} | J^\pi M, E \rangle$ for a given J^π and energy E as

$$\hat{\psi}_E^{J^\pi}(r) = \int r'^2 dr' N^{1/2}(r, r') \langle \Phi(r') | J^\pi, E \rangle \quad \text{with the RGM norm kernel} \quad N(r, r') = \langle \Phi(r) | \Phi(r') \rangle. \quad (8)$$

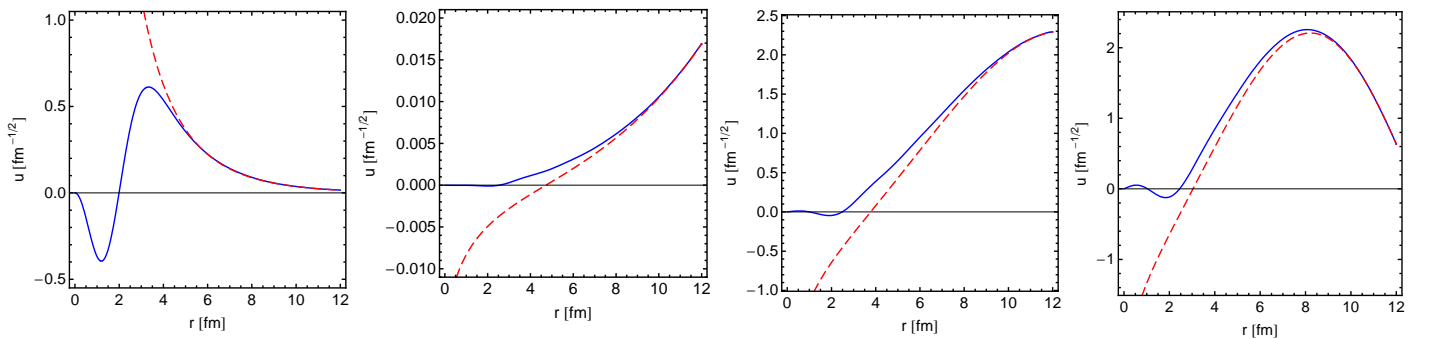


Figure 3: From left to right: overlap functions $r\hat{\psi}_E^{J^\pi}(r)$ for the relative motion of the clusters for the $3/2^-$ ground state and $1/2^+$ scattering states at energies of 0.1 MeV, 1.0 MeV and 2.0 MeV. Dashed lines show the Whittaker and Coulomb functions matched at the channel radius $a=12$ fm, respectively.

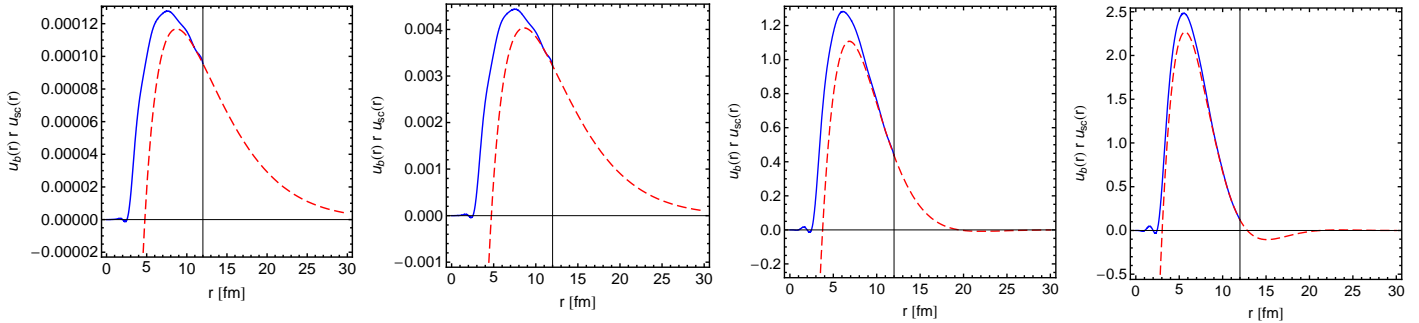


Figure 4: Dipole strength $r\hat{\psi}_{gs}^{3/2-}(r) \cdot r \cdot r\hat{\psi}_E^{1/2+}(r)$ between $3/2^-$ bound state and $1/2^+$ scattering states with energies of 0.05, 0.1, 1.0 and 2.0 MeV. Dashed lines for Whittaker and phase shifted Coulomb functions matched at 12 fm.

Fig. 3 shows three $J^\pi=1/2^+$ scattering overlap functions for different energies and the one for the $J^\pi=3/2^-$ ground state. The dashed lines are the Whittaker function and the phase shifted Coulomb wave functions for scattering and bound states, respectively. When there is no nuclear interaction between the clusters the overlap function has to go over into the Coulomb wave functions. The deviation from the Coulomb solution indicates that the nuclear interaction acts up to 10 fm in the scattering states up to about 6 fm in the more compact ground state. The ground state is an $\ell=1$ state with one node, while the $\ell=0$ scattering states are suppressed in the interior due to the Pauli principle and have two nodes. The $\ell=0$ states with zero and one node are Pauli forbidden and do not exist.

When looking at the dipole strength displayed in Fig. 4 it can be seen that at low energies a large fraction of the dipole matrix element comes from the external region where only the Coulomb force acts. But it should also be noted that even at energies as low as 50 keV we have a significant contribution from the interior region, contrary to common believe that external capture is a good approximation at low energies.

5 Capture Cross Section

At low energies we can restrict ourselves to electric dipole transitions from the S - and D -wave channels. Using the microscopic bound and scattering wave functions and adding up all contributions from the

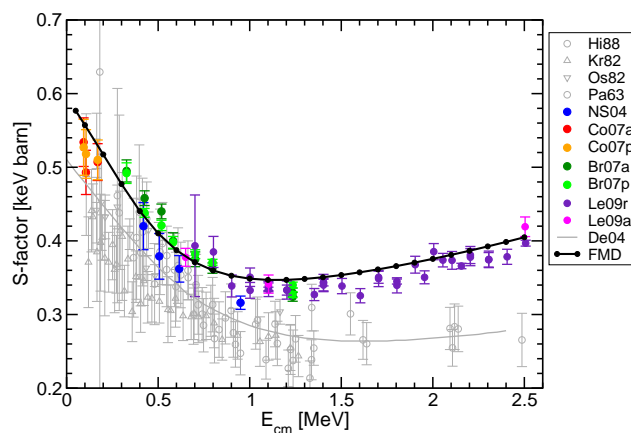


Figure 5: The astrophysical S -factor for the ${}^3\text{He}(\alpha, \gamma){}^7\text{Be}$ reaction. The FMD result is given by the black solid line. Recent data are shown by dark (colored) symbols. Old data are included as gray symbols together with an R -matrix fit.

$J^\pi = 1/2^+, 3/2^+, 5/2^+$ scattering states to the $J^\pi = 3/2^-, 1/2^-$ bound states we calculate the radiative capture cross section which is presented in form of the astrophysical S -factor in Fig. 5. It agrees very well, both in absolute normalization and energy dependence, with the recent experimental results obtained at the Weizmann Institute [25], the LUNA collaboration [26], at Seattle [27] and by the ERNA collaboration [28]. One has to keep in mind that in this *ab initio* approach there are no parameters that can be adjusted to the data. Input are the effective realistic nucleon-nucleon interaction and a suitably chosen many-body Hilbert space.

We also did the corresponding calculation for the ${}^3\text{H}(\alpha,\gamma){}^7\text{Li}$ capture cross sections and found that the measured data are about 15% lower than our calculation, see Fig. 6.

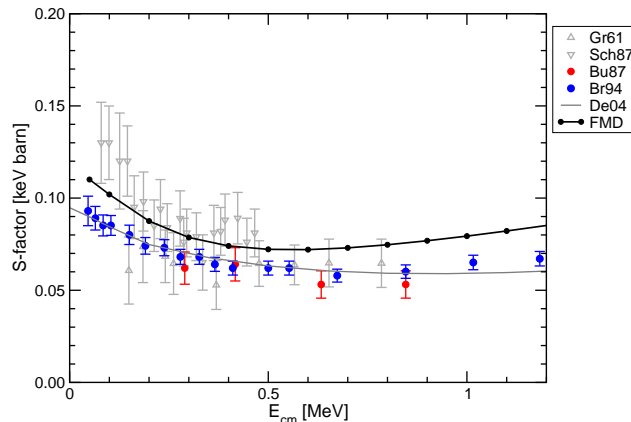


Figure 6: The astrophysical S -factor for the ${}^3\text{H}(\alpha,\gamma){}^7\text{Li}$ reaction. Recent data are shown by dark (colored) symbols together with an R -matrix fit. The FMD result is given by the black solid line. Old data are included as gray symbols.

Future investigations of our results have to reveal why the microscopic FMD model together with a realistic nuclear force describes the data while other models fail. Compared to previous works there are two main differences, the NN-interaction and the many-body Hilbert space. As effective interaction and Hilbert space are strongly correlated we do not expect to identify a single simple reason, like lacking momentum dependence in potential models or too simplified NN-interactions in the microscopic cluster models. It is however clear that one has to include polarized clusters and shell model like ${}^7\text{Be}$ (${}^7\text{Li}$) states in order to get a successful picture. This brings about the very interesting and general question how composite polarizable many-body systems perform quantum tunneling.

References

- [1] T. Neff and H. Feldmeier, Eur. Phys. J Special Topics 156 (2008) 69.
- [2] H. Feldmeier and J. Schnack, Rev. Mod. Phys. 72 (2000) 655.
- [3] H. Feldmeier and J. Schnack, Prog. Part. Nucl. Phys. 39 (1997) 393.
- [4] H. Feldmeier, K. Bieler and J. Schnack, Nucl. Phys. A586 (1995) 493.
- [5] R. Roth, T. Neff and H. Feldmeier, Prog. Part. Nucl. Phys. 65 (2010) 50.
- [6] R. Roth et al., Phys. Rev. C 73 (2006) 044312.
- [7] T. Neff and H. Feldmeier, Nucl. Phys. A713 (2003) 311.

- [8] H. Feldmeier et al., Nucl. Phys. A632 (1998) 61.
- [9] R. Roth et al., Nucl. Phys. A745 (2004) 3.
- [10] M. Chernykh et al., Phys. Rev. Lett. 98 (2007) 032501.
- [11] W. Geithner et al., Phys. Rev. Lett. 101 (2008) 252502.
- [12] B.T. Kim, T. Izumoto and K. Nagatani, Phys. Rev. C 23 (1981) 33.
- [13] P. Mohr, Phys. Rev. C 79 (2009) 065804.
- [14] K. Langanke, Nucl. Phys. A457 (1986) 351.
- [15] T. Kajino, Nucl. Phys. A460 (1986) 559.
- [16] T. Mertelmeier and H.M. Hofmann, Nucl. Phys. A459 (1986) 387.
- [17] A. Csóto and K. Langanke, Few-Body Systems 29 (2000) 121.
- [18] K.M. Nollett, Phys. Rev. C63 (2001) 054002.
- [19] P. Navrátil, C.A. Bertulani and E. Caurier, Nucl. Phys. A787 (2007) 539c.
- [20] K. Langanke, Adv. Nucl. Phys. 21 (1994) 85.
- [21] D. Baye, P.H. Heenen and M. Libert-Heinemann, Nucl. Phys. A291 (1977) 230.
- [22] P. Descouvemont and D. Baye, Rep. Prog. Phys. 73 (2010) 036301.
- [23] W. Nörtershäuser et al., Phys. Rev. Lett. 102 (2009) 062503.
- [24] R.J. Spiger and T.A. Tombrello, Phys. Rev. 163 (1967) 964.
- [25] B.S. Nara Singh et al., Phys. Rev. Lett. 93 (2004) 262503.
- [26] F. Confortola et al., Phys. Rev. C 75 (2007) 065803.
- [27] T.A.D. Brown et al., Phys. Rev. C 76 (2007) 055801.
- [28] A. Di Leva et al., Phys. Rev. Lett. 102 (2009) 232502.

[†] Contribution to the proceedings of the International School of Nuclear Physics, 32nd course, Particle and Nuclear Astrophysics, Erice Sicily, September 16 - 24, 2010.
 To be published in Progress in Nuclear and Particle Physics, Ed. Amand Fäbller.